Simpler and faster quartz crystal microbalance for macromolecule detection using Fixed Frequency Drive

Arnab Guha[1], Niklas Sandström[2], Victor P Ostanin[3], David Klenerman[3], Sourav K Ghosh[1]*
1 Centre for Biological Engineering, Loughborough University, Loughborough, UK
2 Department of Applied Physics, KTH Royal Institute of Technology, Stockholm, Sweden
3 Department of Chemistry, University of Cambridge, Cambridge, UK
* Corresponding author

Abstract

Despite advancements in analytical technologies, their complexity and cost have largely restricted their application in scalable online or multiplexed measurements. Here we report a quartz crystal resonator (QCR)-based method for detection of macromolecules that allows immensely simpler and faster measurements by employing for the first time a fixed frequency drive (FFD) and analytical expressions of acoustic parameters. Using human immunoglobulin E (hIgE) as an exemplar macromolecule and an anti-hIgE aptamer functionalised on a QCR, quantitative accuracy was benchmarked against the traditional impedance analysis method. The ability of FFD to capture data over longer observation periods at significantly higher acquisition rates at a fixed amplitude showed improvement in the QCR's sensitivity and specificity of transduction. The foundations for low-cost and low-power online integration and large-scale multiplexability are also discussed.

Keywords: quartz crystal microbalance (QCM); aptamer; human immunoglobulin E (hIgE); Fixed Frequency Drive (FFD); realtime aptasensor; simple immunosensor; immunoprotein detection

1. Introduction

1.1. Macromolecule Detection

Biomolecular detection is of fundamental interest in life sciences and biotechnology and pivotal in healthcare and pharmaceutical applications. The detection of macromolecules [1] (MW >10 kDa [2]) has gained wide interests in the fields of proteomics [3], diagnostics [1,4], food and bioproduct manufacturing [5], and gene therapy [6,7] due to advancements in analytical techniques [8]. Macromolecules, including antibodies, nucleic acids and exosomes, have been explored as diagnostic markers for diseases, such as cancer [9–11], sepsis [12–14], allergy [15–17], Alzheimer's disease [18–20], tuberculosis [21–23] and cardiovascular disease [24–26]. Macromolecular analysis is also crucial for monitoring the progression of an existing disease [27] and investigating the efficacy of drugs [28]. Cell surface markers, which are largely proteins, execute important biological activities like intercession of cell-cell communications and response to external agents, such as pathogens or chemical messengers [29]. Study of ligand-receptor interactions with other macromolecules like antibodies [30] and aptamers [31], or small molecules, such as molecular imprinted polymers [32] and peptides [33], can reveal important insights into affinity, binding kinetics [34], and conformational changes of macromolecular layers [35].

Conventional analytical techniques for identification and quantification of macromolecules include enzyme linked immunosorbent assay (ELISA) [36], mass spectrometry (MS) [37], nuclear magnetic resonance spectroscopy (NMRS) [38] and surface enhanced Raman spectroscopy (SERS) [39]. While these techniques have allowed unprecedented versatility and accuracy of measurement, the complexity and cost of their instrumentation and assay and the long analysis time have restricted their use to specialised laboratories by skilled operators. To be widely adoptable in clinical and industrial settings, there is a need for simple and low-cost analytical techniques that can deliver rapid or realtime measurements, preferably multiplexable, online or at the point of care in unskilled settings.

Label-free biosensors have the potential to address the above-mentioned need in detection of macromolecules [40–42]. A typical biosensor [31] consists of a biorecognition element or receptor, such as antibody, aptamer, molecular imprinted polymer, peptide or enzyme, that is designed to bind specifically to a target molecule or analyte, and a transduction mechanism that converts the binding event into a detectable signal. Label-free biosensors combine biorecognition and transduction of the binding event in a single step, obviating the need for a secondary molecule or label to read out the binding using additional steps and reagents. Thus, a label-free biosensor can potentially allow a much simpler, faster, cheaper and more scalable detection of macromolecules [43]. Label-free biosensors like surface plasmon resonance (SPR) and electrochemical sensors allow rapid or realtime measurements with increasingly smaller instrument size facilitating portability and scalability [44–46]. However, instrument cost and complexity of SPR sensors and the need for electroactive elements, susceptibility to temperature changes and short shelf life of electrochemical sensors have limited their widescale adoption for online or point-of-care detection of macromolecules [44].

The **quartz crystal resonator (QCR)** has been explored as a label-free sensing platform for macromolecules over the last three decades [47]. A QCR-based biosensor, popularly referred to as the Quartz Crystal Microbalance (QCM), is a thickness-shear mode piezoelectric quartz oscillator with biomolecular receptors functionalised on its sensing electrode [48]. Changes in mass and losses in oscillation energy of the QCR due to any binding or viscoelastic interaction on its sensing electrode are directly measured from the shifts in its resonance frequency and dissipation (resonance half-bandwidth) [49]. The QCR allows versatility through the detection of a broad range of molecular sizes and types regardless of their electrical conductance or optical properties [44]. Since the measurement is label-free and entirely electronic, the QCR serves as a promising platform for rapid or realtime detection of macromolecules. However, in the current state, the technology is not adequately simple and affordable to deliver multiplexed online or point-of-care measurements outside skilled and resourceful laboratory settings.

The **traditional QCR-based methods** for measuring resonance frequency and dissipation include the oscillator circuits [50], impedance or frequency sweep analysis (FS) [51] and ring down or exponential decay [52] methods. The oscillator circuit, comprising a QCR and an amplifier, allows a simple method for determination of resonance frequency using a frequency counter. Dissipation can be measured here but at the expense of simplicity using

an automatic gain control unit. In impedance analysis (or frequency sweep, FS) method, both resonance frequency and dissipation can be estimated by driving the QCR at multiple frequencies around its nominal resonance frequency and fitting the admittance spectra with an equivalent electrical circuit model. In ring down method too, both resonance frequency and dissipation can be measured. A narrow radio frequency pulse excites the QCR in the vicinity of its nominal resonance frequency. The excitation is periodically switched off and the transient QCR response is fitted with the exponential decay function of a damped free oscillation to estimate its resonance frequency and dissipation. However, for both impedance and ring down analysis methods, the requirement for data fitting and averaging limits their measurement time resolution in practice to 0.5-1 sec [53]. The need for frequency synthesizers and fast analog-to-digital converters (ADCs) with a large dynamic range also increases the instrument's complexity, cost, and power consumption, making these methods less suitable for low-cost battery powered instruments. Moreover, the challenges around electromagnetic coupling and the lack of an accurate calibration method to cancel this coupling in a cost-effective way limit large-scale multiplexability of QCRs using these methods.

An analytical formula based Fixed Frequency Drive (FFD) method was reported in our previous work, where we demonstrated realtime detection of quick needle touches on the QCR to study the transient needle-QCR interactions [54]. In this paper, we applied this novel FFD method to report a significantly simpler and faster QCR for truly realtime and continuous label-free detection of a macromolecule, using human immunoglobulin E (hIgE) as an exemplar. The analytical expressions of resonance frequency and dissipation are derived *directly* from the acoustic impedance data based on the Butterworth Van-dyke (BVD) equivalent electrical circuit model of a QCR. Being an analytical expression-based method using a fixed frequency drive, FFD offers greatly improved simplicity and time resolution and can potentially allow enhanced multiplexability and full electronic integration at lower cost and power requirements compared to the traditional impedance and ring down analysis methods.

1.2. Immunoprotein: An exemplar of a macromolecule

The immune system protects the body from infections by producing different immunoproteins or immunoglobulins (Ig). In the field of mammalian immunology, there are five classes of immunoglobulins namely IgA, IgD, IgE, IgG and IgM [55]. Detection of immunoglobulins in human fluids, such as blood, serum and plasma, aids in the diagnosis of hypersensitive reactions [55], infectious disease [56] and allergic disorders [57], to name a few. As an example, IgM and IgG are produced in human blood during the various phases of COVID-19 infection caused by the coronavirus SARS-CoV-2 [56].

Immunoglobulin E (IgE), an immunoprotein with a molecular weight of 190 kDa [58], was used in this work as a model macromolecule. IgE is usually present in trace amounts in the serum of a healthy individual [59]. However, it has the ability to trigger some of the most powerful immune reactions in humans like atopic dermatitis, allergic asthma and other immune deficiency related diseases after being exposed to specific antigens that raises the levels of IgE in human serum [60]. For instance, a correlation between IgE levels and virus

induced asthma aggravation in children and adults are evidenced in the immunology literature [61].

1.3. Human IgE detection: State-of-the-art

Conventional techniques for human IgE detection include the enzyme-linked immunosorbent assay (ELISA) [62], radioallergosorbent test (RAST) [63], microarrays [64], lateral flow test [65], immuno-polymerase chain reaction (IPCR) [66], Matrix-Assisted Laser Desorption-Ionization Mass Spectroscopy (MALDI-MS) [67], flow cytometry [68], electrochemical luminescence (ECL) [60] and immuno-rolling circle amplification (IRCA) [69]. A lot of these tests provide high sensitivity and throughput, but are often time-, skill- and cost-intensive, requiring sample processing steps and a laboratory infrastructure. These features limit their use for rapid point-of-care monitoring of human IgE. Furthermore, some of these methods require labelling of human IgE molecules with enzymes [62], fluorescent molecules [70], magnetic nanoparticles [71] or radioactive elements [64], which may lead to occupancy of the binding site affecting the interaction with the receptor [59].

Label-free IgE detection has been explored using colorimetry [59], surface plasmon resonance (SPR) [72–74], electrochemical impedance spectroscopy (EIS) [75–80], differential pulse voltammetry (DPV) [81], field effect transistors (FET) [73,82–86], quartz crystal resonator (QCR) [57,58,72,87–91], thin film bulk acoustic resonator (FBAR) [15], surface acoustic wave (SAW) [92,93], and flexural plate wave (FPW) sensors [55,94], employing antibody or aptamer receptors. Most of these methods show promising results in sensitivity and quantification of human IgE but have challenges for simple, low-cost and in-situ or online measurements. SPR is limited in terms of complexity and cost of instrumentation, while the need for electroactive receptor probe [95] and set-up complexities [96] challenge the fabrication of miniaturised electrochemical sensors.

Acoustic sensors, such as QCR, FBAR, SAW and FPW, are entirely electronic and have fundamental merits in addressing the need for rapid point-of-care sensors for macromolecules like IgE. FBAR, SAW and FPW sensors have been used for human IgE detection. These methods are accurate but require complex instrumentation and data fitting. Till date, only 8 journal articles have reported QCR-based detection of human IgE, all of them using oscillator circuits [57,58,72,87–91]. Although oscillator circuits are simple and inexpensive, they are limited in terms of tracking accuracy due to the influence of circuit components on sensor response [97]. Measurement of dissipation shifts with addition of an automatic gain control unit also compromises simplicity of oscillator circuits. Frequency sweep and ring down based QCR methods have not been reported for IgE detection. Nevertheless, like FBAR and SAW, although accurate, the complexity of instrumentation associated with these QCR methods are still unsuitable for simple and low-cost battery powered devices for point-of-care or online multiplexed measurements.

In this work, for the first time, we combined simplicity and accuracy through the application of fixed frequency drive (FFD) to demonstrate label-free, realtime, and quantitative detection of human IgE (hIgE). The frequency shifts obtained using the FFD method agreed satisfactorily with that obtained using the impedance analysis method. The potential for

greater sensitivity due to lower baseline noise, superior time resolution, multiplexability and online integration features have also been discussed here in the context of macromolecule detection. An anti-hIgE aptamer was used as receptor instead of an antibody due to lower cost of manufacturing and greater specificity, stability, and shelf life of aptamers. Our literature review revealed the various aptamers used for IgE detection [58–60,64,67,70,73–76,78–86,89,91,98–104]. Among these, we noted different versions of D17.4 anti-hIgE aptamer to be well characterised and validated for label-free human IgE detection [73,89]. We employed one version of D17.4 anti-hIgE aptamer in this work [105]. Human immunoglobulin-G (hIgG) was used as a negative control.

2. Materials and Methods

2.1. Fixed Frequency Drive (FFD) Method

Method for resonance frequency shift measurement

Analytical expressions for resonance frequency and dissipation of the QCR were derived as a function of its acoustic (or motional) impedance using a novel analytical approach. The QCR was modelled as a mechanical oscillator consisting of mass (m), spring (of spring constant k) and damper (with damping coefficient c) (**Fig. 1a**). The Butterworth Van-dyke (BVD) equivalent electrical circuit model for this mechanical oscillator is shown in **Fig. 1b** [106]. The motional arm of this equivalent circuit comprises a resistor (R_m), an inductor (L_m) and a capacitor (C_m), which represent equivalence to the viscous damping coefficient (c), mass (m) and shear compliance (inverse of spring constant, $1/k$) of the mechanical oscillator, respectively. The other arm of the equivalent circuit, comprising the shunt capacitance (C_s), represents the parasitic electrical capacitance between the QCR electrodes and the holder capacitance.

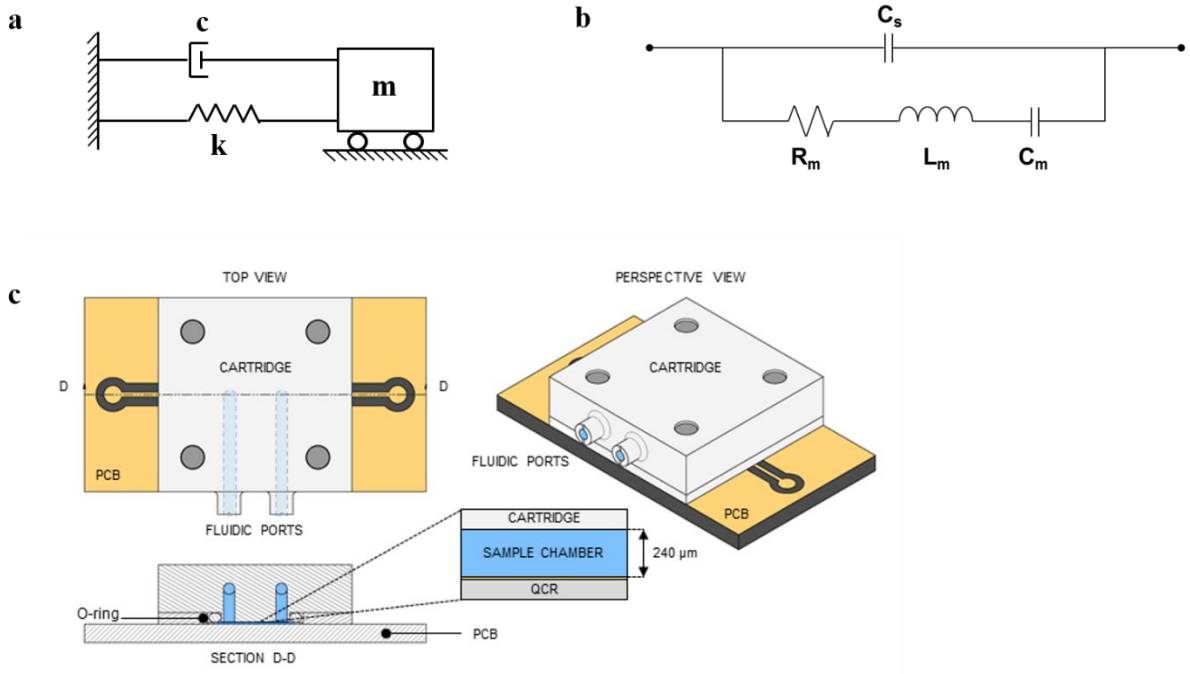

Fig. 1. **a.** Mechanical oscillator model of a quartz crystal resonator (QCR). **b.** Butterworth Van Dyke (BVD) equivalent circuit diagram for a QCR. **c.** QCR sensor assembled with a printed circuit board and a microfluidic cartridge.

The reactance (imaginary component of complex impedance) of the motional arm of the equivalent circuit is given by Eq. 1, where $\omega = 2\pi f$ is the frequency at which the QCR is driven (drive frequency).

$$X_m = \omega L_m - \frac{1}{\omega C_m} \tag{1}$$

The angular resonance frequency and the characteristic shear wave impedance of the QCR are given by $\omega_0 = 1/\sqrt{L_m C_m}$ and $\rho = \sqrt{L_m/C_m}$ respectively. Using these two expressions, the motional inductance and motional capacitance can also be expressed as $L_m = \frac{\rho}{\omega_0}$ and $C_m = \frac{1}{\rho\omega_0}$ respectively. Replacing these parameters in Eq. 1 gives the alternative expression of motional reactance (Eq. 2).

$$X_m = \rho\left(\frac{\omega}{\omega_0} - \frac{\omega_0}{\omega}\right) = \rho\left(\frac{f}{f_0} - \frac{f_0}{f}\right) \tag{2}$$

$$\Rightarrow \frac{\rho}{f}{f_0}^2 + X_m f_0 - \rho f = 0 \tag{3}$$

The analytical expression of the QCR's resonance frequency ($f_0 = \frac{\omega_0}{2\pi}$) is obtained from the solution of Eq. 3 as follows.

$$f_0 = \frac{f}{2\rho}\left(-X_m + \sqrt{{X_m}^2 + 4\rho^2}\right) \tag{4}$$

The resonance frequency of the QCR shifts as molecular binding occurs on its electrode causing a change in the oscillator mass. If the drive frequency (f) is set to the initial resonance frequency of the QCR, i.e., the resonance frequency before the start of binding, the resonance frequency shift at any point in time during binding can be given using Eq. 4 by

$$\Delta f_0 = f_0 - f = \frac{-f}{2\rho}\left(X_m + 2\rho - \sqrt{{X_m}^2 + 4\rho^2}\right) \tag{5}$$

Eq. 5 can be expressed alternatively as follows.

$$\Delta f_0 = -f\frac{X_m}{2\rho}\left(1 - \frac{\frac{X_m}{2\rho}}{1 + \sqrt{1 + \left(\frac{X_m}{2\rho}\right)^2}}\right) \tag{6}$$

To get a quantitative estimate of $\frac{X_m}{2\rho}$, Eq. 2 can be alternatively expressed as follows.

$$\frac{X_m}{\rho} = \frac{f^2 - {f_0}^2}{f f_0} \tag{7}$$

$$\Rightarrow \frac{X_m}{\rho} = \frac{(f - f_0)(f + f_0)}{f f_0} = -\frac{\Delta f_0 (f + f_0)}{f f_0}$$

$$\Rightarrow \frac{X_m}{2\rho} = -\frac{1}{2}\left(\frac{\Delta f_0}{f} + \frac{\Delta f_0}{f_0}\right)$$

The resonance frequency (f_0) of most QCRs is in the range of 5-30 MHz, and in FFD, the drive frequency is set to the initial resonance frequency (i.e., resonance frequency before any binding). The resonance frequency shift, on the other hand, is typically in the range of ~100 Hz - 1 kHz for most biomolecular binding. Thus, from Eq. 7 one can see that $\frac{X_m}{2\rho}$ is a very small fraction, in the range of ~10^{-5} - 10^{-4}. Hence, the second order Maclaurin series approximation of Eq. 6, as presented in Eq. 8, gives a simple but adequately accurate expression of resonance frequency shift.

$$\Delta f_0 = -f \frac{X_m}{2\rho}\left(1 - \frac{1}{2}\frac{X_m}{2\rho}\right) \tag{8}$$

The reactance is determined from the experimentally measured impedance (Z) after cancelling the current through the shunt capacitance (C_s) as $X_m = Im((1/Z - j\omega C_s)^{-1})$. The shunt capacitance, which represents the parasitic electrical capacitance between the QCR electrodes and the holder capacitance, does not vary with binding. The characteristic wave impedance (ρ) can also be considered to be practically constant as its relative shift is very small. The relative shift in ρ for molecular binding, where $\rho = \sqrt{L_m/C_m}$, can be expressed as $\Delta\rho/\rho = -\Delta f_0/f_0$ as addition of mass (change in L_m) is dominant here and change in stiffness (change in $1/C_m$) is negligible. For the IgE binding experiments reported here, $\Delta\rho/\rho \sim 2.1 \times 10^{-5}$. Thus, characteristic wave impedance and shunt capacitance can be measured once for a batch of crystals and used unchanged to evaluate the resonance frequency shifts due to molecular binding using Eq. 6 or Eq. 8. These equations allow the determination of resonance frequency shift corresponding to each measured impedance data point directly in realtime *without the need for any data fitting*. Besides simplicity, this fixed frequency drive (FFD) method of resonance frequency shift determination also offers the potential for a high time resolution of measurement as discussed in this paper.

Method for dissipation measurement

The energy dissipation of a QCR is due to viscous damping at its sample interface. For biosensing applications, the damping is predominantly due to the sample liquid although biological cells can also contribute to damping. The dissipation is represented by the resonance half-bandwidth (Γ). The quality factor (Q) of a QCR is defined as the ratio of the resonance frequency and the resonance bandwidth (2Γ) as follows.

$$Q = \frac{f_0}{2\Gamma} \tag{9}$$

In terms of the equivalent electrical circuit, the quality factor of a QCR is given as follows.

$$Q = 2\pi \times \frac{\text{Energy Stored}}{\text{Energy Lost Over 1 Period}} \tag{10}$$

$$\Rightarrow Q = \frac{2\pi \times \frac{L_m {i_{max}}^2}{2}}{R_m {i_{rms}}^2 \times \frac{2\pi}{\omega_0}}$$

$$\Rightarrow Q = \frac{2\pi \times \frac{L_m {i_{max}}^2}{2}}{\frac{R_m {i_{max}}^2}{2} \times \frac{2\pi}{\omega_0}} = \frac{\omega_0 L_m}{R_m}$$

$$\Rightarrow Q = \frac{\rho}{R_m} \tag{11}$$

Equating Eq. 9 and Eq. 11, we get the expression of dissipation of the QCR as follows.

$$\Gamma = \frac{f_0 R_m}{2\rho} \tag{12}$$

The motional resistance can be determined from the measured impedance as $R_m = Re((1/Z - j\omega C_s)^{-1})$. The resonance frequency, $f_0 = f + \Delta f_0$, can be determined using the resonance frequency shift (Δf_0) estimated using Eq. 6 or Eq. 8 and the characteristic wave impedance is practically constant for a batch of crystals as discussed earlier. Thus, the dissipation of the QCR can be determined corresponding to each measured impedance data point directly in realtime using Eq. 12 *without the need for any data fitting* similar to resonance frequency shifts. The dissipation data was not included in this paper as IgE binding was found to contribute negligibly to the dissipation of QCR. This can be explained by the fact that IgE molecules are coupled reasonably tightly with the QCR motion due to its small size (~7 nm) relative to the acoustic penetration depth of a 14.3 MHz QCR with one side exposed to liquid (~150 nm) [107].

2.2. Reagents

Acetone, isopropanol, ultra-pure 200-proof ethanol, phosphate buffered saline (PBS) and streptavidin were purchased from Sigma-Aldrich (UK). The PBS (pH 7.4) contained 8.1 mM Na_2HPO_4, 1.1 mM KH_2PO_4, 1 mM $MgCl_2$, 2.7 mM KCl, and 138 mM NaCl. Deionised (DI) water was obtained from Milli-Q Integral Water Purification Systems (Millipore, USA). Human immunoglobulin-E (hIgE) (ab65866) and human immunoglobulin-G (hIgG) (ab91102) were procured from Abcam (Cambridge, UK). D17.4 biotinylated anti-hIgE aptamer (MW=19.0234 kDa) with a base sequence of 5'-GGG GCA CGT TTA TCC GTC CCT CCT AGT GGC GTG CCC CTT TTT TTT TTT TTT TTT TTT TTT T/3Bio/-3' was synthesised by Integrated DNA Technologies (IDT) [105]. Thiolated alkanes, HS-(CH_2)11-EG6-Biotin and HS-(CH_2)11-EG3-OCH_3, were purchased from ProChimia (Poland).

2.3. Quartz crystal resonator (QCR)

14.3 MHz AT-cut thickness shear mode quartz crystal resonators were procured from Laptech Precision Inc., Bowmanville, Ontario, Canada. The diameter and thickness of the blank crystals were 8.3 mm and 115 µm, respectively. The quartz substrate was sandwiched between two circular gold electrodes, Ø 5 mm on the top and Ø 4 mm on the bottom. The

top electrode wrapped around the crystal edge to the bottom side to allow electrical connections from the bottom side, isolated from the sample on the top side.

2.4. Cleaning of QCR

The QCR was placed in a Petri dish and cleaned using ultrasonication in acetone for 5 min and thereafter ultrasonication in isopropanol for 10 min. The QCR was then dried using a flow of nitrogen gas and finally treated in argon plasma at 30 W for 45 sec employing a Harrick Plasma Cleaner.

2.5. QCR functionalisation with a self-assembled monolayer (SAM) of thiols

The cleaned QCR was kept in a 24-well plate and incubated in 250 μL 1 mM ethanolic solution of a thiol mixture comprising 10% biotin thiol (HS-(CH_2)11-EG6-Biotin) and 90% methoxy thiol (HS-(CH_2)11-EG3-OCH_3) by volume for approximately 18 hours to allow the formation of a mixed self-assembled monolayer (SAM) of thiols over the QCR surface. The methoxy thiol was used as a filler to reduce the steric hindrance from a dense packing of pure biotin thiol. After 18 hours, unbound thiols were removed by a series of ethanol and DI water washes.

2.6. Sensor assembly

SAM-functionalised QCR was dried using nitrogen gas and subsequently assembled between a microfluidic cartridge on the top and a printed circuit board (PCB) on the bottom (**Fig. 1c**). The microfluidic cartridge was fabricated by precision milling of an acrylic substrate and used to deliver the sample onto the QCR. The PCB provided the electrical connections to the bottom of the QCR. A UPS VI classified EPDM O-ring (Trelleborg AB, Sweden) was fitted underneath the microfluidic cartridge to create a sealed sample space of ~13 μL on the QCR. The complete assembly was held together by a pair of clips (not shown in Fig. 1c). A quality factor of ~1900 was achieved for the assembled QCR sensor under liquid, confirming insignificant damping from the O-ring.

2.7. Immobilisation of biotinylated anti-human-IgE aptamer on QCR

After establishing the sensing assembly, 1 mL of DI water (at 100 μL/min for 10 min) and 0.8 mL of PBS (at 40 μL/min for 20 min) were flowed successively to stabilise the resonance frequency. Streptavidin solution (2.5 μg/mL in PBS) was then injected into the sensor assembly at 40 μL/min for 15 min to allow the binding of streptavidin with biotin of the mixed SAM layer on the QCR. The anti-hIgE aptamer stock solution (0.2 μM in PBS) was denatured by heating at 95 °C for 5 min and subsequently cooled for 20 min at room temperature before being injected into the sensor assembly at 40 μL/min. The biotinylated aptamer was captured on the QCR through binding of its biotin end with the streptavidin captured on the QCR in the previous step. **Fig. 2d** shows the design of the QCR biosensor surface.

2.8. Experimental set-up

A custom-built network analyser with PC-based graphical user interface control and a facility to drive at a wide range of frequency and amplitude was employed for actuating and sensing

the QCR [105,108]. Wolfram Mathematica 10 was used for processing the experimental data. A controlled and measured injection of sample into the QCR sensor module was achieved using a Harvard Apparatus syringe pump.

3. Experimental Results

3.1. Quantitative validation of FFD method against impedance analysis method

The fixed frequency drive (FFD) method for hIgE detection was first validated quantitatively against the traditional impedance analysis (or frequency sweep, FS) method. A frequency modulation scan (central frequency: 14.3 MHz, span: 20 kHz, amplitude: 0.1 V, duration: 10 sec) and a fixed-frequency-and-amplitude scan (frequency: 14.3 MHz, amplitude: 0.1 V, duration: 10 sec), representing the impedance analysis and FFD methods respectively, were taken successively at a gap of 3 sec and repeated over 5 min of blank PBS solution flow (at 40 µL/min) to establish a resonance frequency baseline, and over 30 min of hIgE solution flow (at 40 µL/min) to measure the resonance frequency shift due to hIgE binding with anti-hIgE aptamer on the QCR. A range of hIgE concentrations was explored (0 nM, 2.63 nM, 5.26 nM, and 10.53 nM). Separate experiments were conducted for each hIgE concentration employing separate QCRs. As mass coupling is the dominant phenomenon in hIgE binding and dissipation changes are negligible, as explained in Section 2.1, the resonance frequency shifts recorded from these experiments can be attributed to the mass of hIgE binding following the Sauerbrey equation ($\Delta m/m = -\Delta f_0/f_0$) [109].

For impedance analysis method, the admittance (inverse of impedance) spectrum from each 10 sec frequency sweep was fitted with the BVD model to determine the parameters of the equivalent circuit (**Fig. 1b**) (Section 2.1). These parameters were then used to evaluate the resonance frequency from definition as $f_0 = 1/(2\pi\sqrt{L_m C_m})$. The resonance frequency shift corresponding to each frequency sweep was thus recorded over the baseline and binding phases with reference to the first baseline resonance frequency reading (**Fig. 2a**).

For FFD method, impedance datapoints (X_m) were captured at a rate of 30518 points/sec (or 30.518 kHz) over a 10 sec fixed-frequency-and-amplitude scan. To limit the size of the output file, moving average was applied to write only 1192 datapoints into the file for every 10 sec scan, i.e., one datapoint every 8.39 ms. The resonance frequency shift corresponding to each impedance datapoint was determined by applying Eq. 6. To allow comparison with impedance analysis method, the 1192 resonance shift values thus obtained from each scan were averaged to derive one value for every 10 sec scan. The resonance frequency shifts thus derived were recorded over the baseline and binding phases with reference to the first baseline reading (**Fig. 2a**).

A satisfactory quantitative agreement was observed between the two methods for all the resonance frequency shifts over the baseline and hIgE binding phases for all the concentrations (**Fig. 2a**). The baseline noise (standard deviation) for FFD and impedance analysis methods were also comparable at 2.37 Hz and 2.38 Hz, respectively. The low baseline noise from the sensor can be attributed to a high-quality surface preparation and low instrument noise. An average resonance frequency drift of ~20 Hz was observed over 35 min of blank PBS solution flow (0 nM hIgE in **Fig. 2a**), which limited the exploration of

hIgE concentrations below 2.63 nM using this set-up. This drift can be attributed primarily to temperature variation and should be addressable using a temperature stabiliser. An encouraging quantitative agreement was observed between the final resonance frequency shifts estimated for each concentration using the two methods: the FFD frequency shifts were within -2.09% to 1.15% of the corresponding impedance analysis frequency shifts across the hIgE concentration range (**Fig. 2b**) and showed a linear correlation with the concentrations (R^2 = 0.9675), abiding by the Sauerbrey equation ($\Delta f_0 \propto \Delta m$) (**Fig. 2c**).

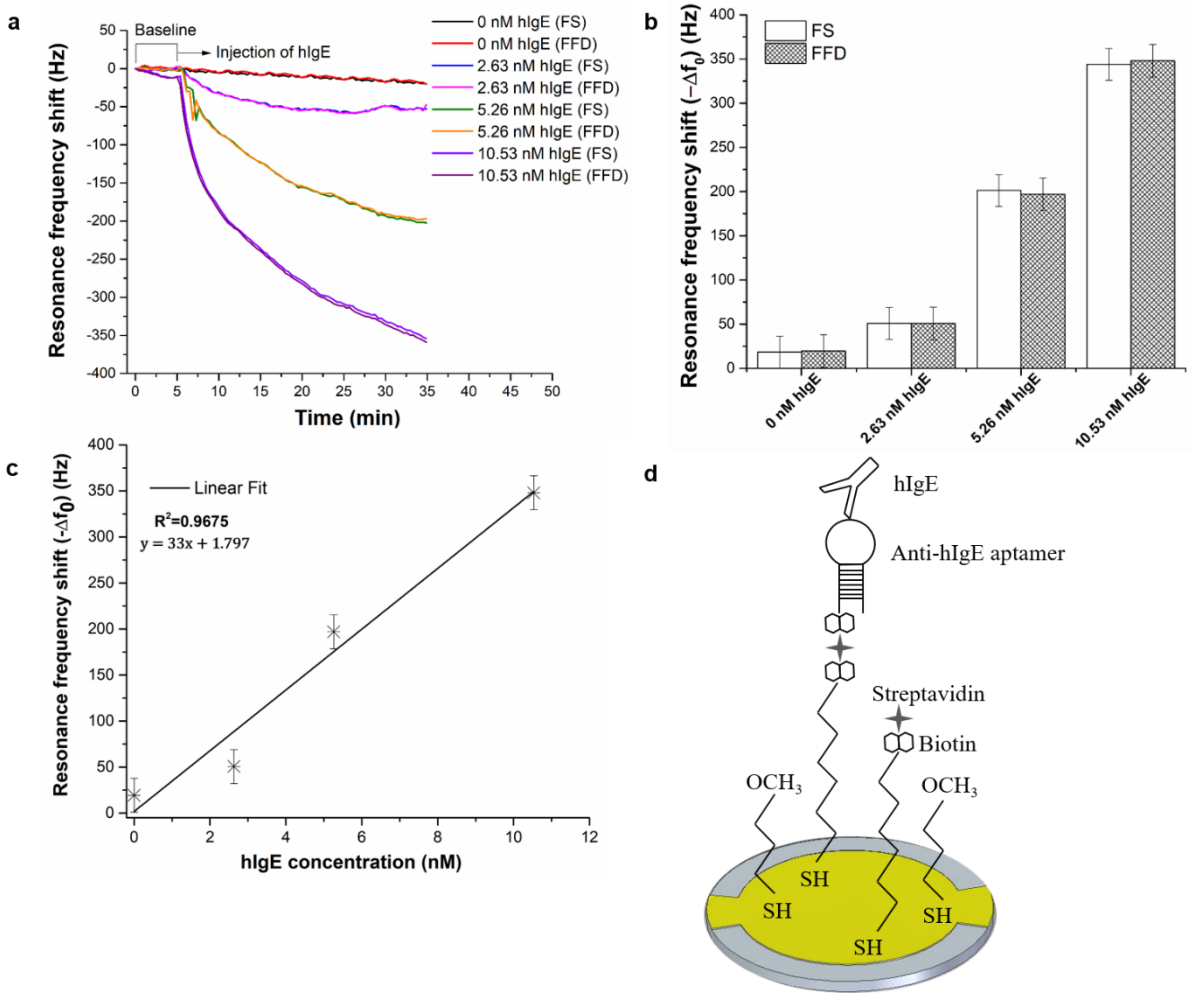

Fig. 2. a. Resonance frequency shifts over the baselining (5 min) and binding (30 min) phases for various hIgE concentrations using fixed frequency drive (FFD) and impedance analysis (or frequency sweep, FS) methods. **b**. Comparison of resonance frequency shifts 30 min after injection of various hIgE concentrations estimated using the two methods. **c.** The linear correlation of the final resonance frequency shifts using FFD with hIgE concentrations (R^2 = 0.9675). **d.** The QCR biosensor surface design.

3.2. Realtime detection of hIgE employing FFD in continuous scan mode

The FFD method was next explored for realtime detection of hIgE. A 14.3 MHz QCR was functionalised with biotinylated anti-hIgE aptamer (as in Section 2.7). PBS buffer was flowed over the QCR (at 40 µL/min) to stabilise its resonance frequency. A single fixed-frequency-

and-amplitude scan of 0.5 V was then taken for a duration of 60 min. This single scan is referred to as “continuous FFD mode” as impedance datapoints were captured in realtime throughout the scan at an acquisition rate of 30.518 kHz. To limit the output file size, moving average was applied to finally record 15674 datapoints for a 60 min scan, i.e., one datapoint every 229.68 ms. Resonance frequency shift was derived corresponding to each of these datapoints by applying Eq. 6. Blank PBS was flowed over the QCR (at 40 µL/min) for the first 30 min of the scan to record a resonance frequency baseline after which hIgE was spiked in the flowing PBS buffer to record the binding phase. A range of hIgE concentrations (from 2.63 nM to 21.06 nM) was explored (**Fig. 3a**). Specificity of detection was investigated using human immunoglobulin G (hIgG) as a negative control at a concentration of 21.06 nM, which was the highest hIgE concentration explored. Separate QCRs were employed for each experiment. A twofold lower baseline noise (standard deviation, 1.3 Hz) was observed for continuous FFD compared to the impedance analysis method over a 5 min baseline duration, although the same instrument, sensor surface, and assay design were used for both the methods. This may be explained by the fact that the entire 5 min (or 300 sec) baseline was the period of observation for the continuous FFD scan (in Section 3.2), whereas for the 14 frequency sweep scans (of 10 sec each) that were performed over the 5 min baseline in the impedance analysis method (in Section 3.1), the period of observation was only 140 sec. Moreover, the QCR oscillation amplitude varied over a single frequency sweep of the impedance analysis method. The oscillation amplitude was lower when the drive frequency was farther from the resonance frequency and went higher as the drive frequency approached the resonance frequency. The oscillation amplitude at the start and end of the 20 kHz frequency sweep span was nearly zero as the resonance bandwidth (7.5 kHz for a 14.3 MHz QCR with 1900 quality factor) was much smaller than the span. The oscillation amplitude (a) near the resonance can be estimated using $a = 1.25QV_d$ [110] as 0.24 nm for a quality factor (Q) of 1900 and drive voltage (V_d) of 0.1 V. On the other hand, the oscillation amplitude remained constant at ~0.24 nm in the continuous FFD scan as the drive frequency remained constant and close to the resonance frequency, whose shift (<350 Hz) was negligible compared to the resonance bandwidth (7.5 kHz). Varying oscillation amplitude in the frequency sweep could potentially allow loosely bound species to settle down on the QCR surface during the low amplitude phase of the scan and come off the surface randomly during the high amplitude phase close to resonance, contributing to additional noise.

The resonance frequency shifts relative to the baseline obtained at the end of the 30 min binding phase for the hIgE samples had a quantitative correlation with the hIgE concentrations whereas the shift from the 21.06 nM hIgG sample (-19.56 Hz in 30 min) was negligible and nearly equal to the frequency drift of ~25 Hz in 35 min (**Fig. 3b**). The frequency shifts (after drift correction) for the hIgE samples had a satisfactory linear fit with the hIgE concentrations (R^2 = 0.9932), once again agreeing with the Sauerbrey equation (**Fig. 3c**).

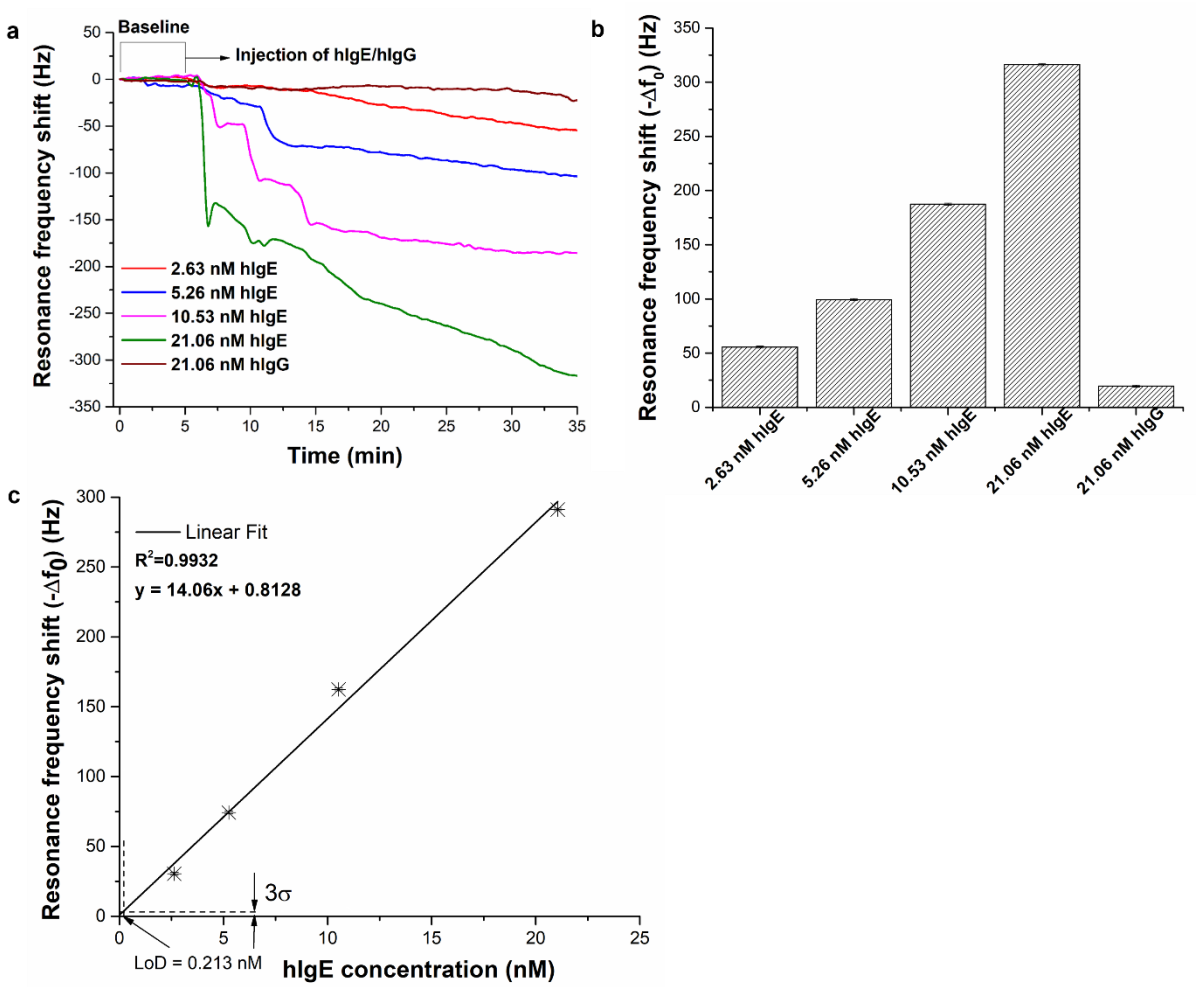

Fig. 3. Results from continuous FFD mode scan a. Realtime resonance frequency shifts due to hIgE and hIgG binding. **b**. The resonance frequency shifts recorded at the end of the 30 min binding phase of hIgE and hIgG. **c.** Linear correlation of the resonance frequency shifts (after drift correction) with hIgE concentrations and estimation of limit of detection (LoD). σ represents the standard deviation of the baseline.

We note from **Fig. 3a** that the hIgE binding curves for higher hIgE concentrations (>5.26 nM) show multiple jumps that are not visible for lower concentrations. These jumps were not observed with the intermittent FFD scan experiment either (**Fig 2a**). We hypothesise that for higher hIgE concentrations, there is an increased steric hindrance on the QCR surface from neighbouring hIgE molecules that causes some hIgE molecules to bind weakly with the sensor surface. The activation energy of these interactions is further lowered under the influence of the pulling force exerted by the oscillating QCR, a phenomenon that is well known [111]. There is a greater probability of dissociation of these weaker interactions mediated by “giant thermal fluctuations” (as defined in Arrhenius- Boltzmann-Eyring theory) in the continuous mode FFD experiments due to the longer scan time (one scan: 1800 sec) compared to the intermittent mode FFD experiments (one scan: 10 sec) [112]. We anticipate that these random dissociations of the weaker hIgE interactions are reflected as jumps in the realtime resonance frequency shift curves for higher hIgE concentrations (**Fig. 3a**).

4. Discussion

4.1. Sensitivity of detection

The sensitivity is influenced by several factors including the detection method, affinity of receptor, the instrument set-up, the assay design and the quality of sensor surface preparation. Although optimising the sensitivity was not the objective of this work, encouraging limit of detection was estimated with the current sensor set-up. Correcting for the resonance frequency drift, and setting the minimum detectable signal at 3σ, where σ = 1 Hz is the standard deviation of the 30 min baseline, the limit of detection (LoD) using continuous scan FFD method was estimated at 213 pM. One important factor behind this low LoD is the ability to record resonance frequency shifts continuously at a high speed (30.518 kHz) through a long scan, and then averaging as needed, to achieve low noise. The fixed oscillation amplitude of the QCR also avoids random settling and unsettling of loosely bound species on the surface, which helps in reducing noise. Besides the detection method, the method of biosensor preparation with the QCR assembled within the microfluidic cell (**Fig. 1c**) allowed a controlled surface functionalisation process and monitoring of the same using the QCR. Moreover, the D17.4 anti-hIgE aptamer employed here was thoroughly validated in our earlier work for sensitive hIgE detection with low cross-reactivity [105].

4.2. Specificity of detection

Human Immunoglobulin G (hIgG) (MW: 150 kDa) was selected as the negative control for non-specific binding study using the continuous mode FFD scan experiments as described in Section 3.2. The resonance frequency shift after 30 min of 21.06 nM hIgG binding (-19.56 Hz) was ~16 times lower than that for similar duration and concentration of hIgE binding (-316.2 Hz) (**Fig. 3b**). Besides the high-affinity and low cross-reactivity aptamer, we anticipate the continuous fluid flow and fixed amplitude QCR oscillation also played a role in the high specificity of detection by dissociating non-specific interactions.

The sensitivity and specificity can be further improved through optimisation. The drift can be reduced to a large extent by integrating a thermal regulator within the microfluidic cartridge. The Sauerbrey equation suggests that QCR sensitivity per unit area varies as square of its fundamental resonance frequency albeit at the expense of quality factor [113]. It will be worth exploring mesa crystals with higher fundamental resonance frequencies, such as 50 MHz or 100 MHz, to study the influence of higher drive frequency on resonance frequency shift resolution, which governs the LoD. The sensitivity and specificity can also be improved by optimising the sensor surface and assay design, such as buffer composition, blockers, and aptamer concentration. A recent study reported the influence of electrode material on QCR mass sensitivity, which may be explored using FFD method [114]. Moreover, the QCR mass sensitivity varies nonuniformly across its diameter, which restricts the quantitative accuracy and LoD. Uniform mass sensitivity across the QCR diameter can be aimed for by employing a ring electrode with optimised inner and outer radii. This may lead to enhanced quantitative accuracy and LoD of this FFD-based QCR method [115].

4.3. Time Resolution

Since the FFD method can estimate the shifts in resonance frequency and dissipation directly from the measured impedance data using analytical expressions, these acoustic

shifts can potentially be recorded as fast as the data acquisition rate of the instrument. The accuracy of these readings may be affected where the decay time ($Q/(\pi f_0)$) of QCR transient oscillations is comparable with the instrument's period of data acquisition. For example, the decay time for our 14.3 MHz QCR with a quality factor of 2000 in liquid is 44.5 µs, whereas the period of data acquisition for our instrument with an acquisition rate of 30.518 kHz is 32.76 µs. So, the time resolution for this set-up will be slightly higher than the period of data acquisition. However, where the decay time is considerably lower than the instrument's period of data acquisition, such as for a QCR with higher fundamental resonance frequency that has a lower quality factor, the measurement time resolution is primarily governed by the latter. Thus, with an appropriate selection of QCR fundamental resonance frequency, it is possible to achieve a time resolution of 32.76 µs using the current instrument and FFD method, which is nearly 3 orders of magnitude better than the fastest QCR instruments reported [53]. Thus, the FFD method can bring a paradigm change in the speed of acoustic shift measurements, enabling truly realtime measurements using relatively simple and low-cost instrumentation. Sub-millisecond time resolution will potentially allow the study of transient biomolecular processes, such as protein-DNA and protein-ligand interactions and protein folding [116,117]. Where there is no need for such an ultrahigh time resolution, moving average can be applied on the data. This will lower the time resolution but improve the limit of detection by cancelling out normal additive noise.

4.4. Online Integration

Online integration of acoustic sensors is essential to enable their widescale adoption in diagnostics and manufacturing industry. The frequency sweep [118] and oscillator circuit [119] methods have been explored for implementation of QCR on printed circuit boards. An integrated circuit was also reported for estimation of QCR dissipation factor using ring down method [120]. As the resonance frequency and dissipation can be determined in realtime in FFD using analytical expression and a fixed frequency and fixed amplitude drive, this method potentially allows full electronic integration of QCR with much less complexity, cost and power consumption. The intrinsic high time resolution of the method obviates the need for a fast analog-to-digital converter. With no need for frequency modulation, the frequency synthesizer can also be replaced with a self-oscillating QCR to drive the sensing QCR at a fixed frequency and amplitude.

4.5. Multiplexability

Multiplexability, i.e., the capability to read multiple QCRs, is often a desired QCR feature where multiple targets or biomarkers need to be measured at the same time. Impedance analysis, ring down, and oscillator circuit techniques have been explored for multiplexability [121–135]. QCRs can be driven in series using electronic switches but the associated complexity limits the degree of multiplexability. In most cases, multiple QCR oscillators are fabricated on a single piece of quartz substrate, referred to as multi-channel monolithic quartz crystal microbalance (MQCM). Each QCR oscillator of the MQCM is driven in parallel by separate driver circuits and their outputs are synchronised using a central processing unit. This makes the integrated electronic circuit bulky and difficult to multiplex. Moreover, MQCMs are affected by acoustic and electromagnetic couplings between the adjacent QCRs that need to be

addressed to ensure accuracy of readings. The acoustic coupling can be suppressed in various ways, such as using an inverted mesa quartz substrate [126], insertion of polydimethylsiloxane (PDMS) wall between adjacent QCR oscillators [126], or maintaining a certain distance between them [124]. The suppression of electromagnetic coupling is more complex and requires expensive shielding, which limits the degree of multiplexability. Spurious electromagnetic coupling can be eliminated to a large extent during data processing using prior calibration. However, calibration can be cumbersome for impedance analysis method as the MQCM device needs to be calibrated for each frequency within the drive frequency span. Cancelling electromagnetic coupling using calibration is immensely more problematic for oscillator circuit and ring-down methods and there is no calibration procedure reported in the current literature. In contrast, calibration is uniquely feasible for FFD method as the device needs to be calibrated for one frequency only and can offer a promising way to achieve a higher degree of multiplexability at low cost, complexity, and power requirements.

5. Conclusion

The paper reports a novel quartz crystal resonator-based method for detection of macromolecules with significantly greater simplicity and measurement speed than the traditional methods taking human immunoglobulin E (hIgE) as a model macromolecule. The use of a fixed frequency drive (FFD) and analytical expressions to derive the acoustic shifts directly from the impedance data underpin the method's enhanced simplicity and time resolution (up to 32.76 μs). The satisfactory quantitative agreement of the resonance frequency shifts with impedance analysis method and their linear correlation with hIgE concentrations demonstrate the accuracy of FFD method. The ability to record acoustic shift data over longer observation periods at high speed that can be averaged to reduce noise enables lower limits of detection. The "acoustic cleaning" of the QCR surface of weakly bound species with a continuous fixed amplitude scan further reduces noise and non-specific binding. The simplicity and single frequency drive provide a strong foundation for low-cost and low-power online integration and large-scale multiplexability, which are crucial for wider industrial adoption of the QCR and warrant further investigation. It will also be worth exploring the FFD method for detection of other biomolecules and biological particles with suitable choice of bioreceptor and drive frequency.

Acknowledgements

The authors are thankful to Dr Alexander Zhukov of University of Cambridge for his contributions to the enhancement of the graphical user interface of the custom-built network analyser instrument used here. The authors also acknowledge the contributions of EU projects RAPP-ID (FP7-JTI 115153) and Norosensor (FP7-NMP 604244), and the EPSRC Bridging the Gap in Antimicrobial Resistance grant (EP/M027341/1) for covering the cost of instrument development and consumables, and the Doctoral College of Loughborough University for supporting the PhD studentship of Dr Arnab Guha.

References

[1] M. Jia, S. Li, L. Zang, X. Lu, H. Zhang, Analysis of biomolecules based on the surface enhanced raman spectroscopy, Nanomaterials. 8 (2018) 1–27.

https://doi.org/10.3390/nano8090730.
[2] A. Syahir, K. Usui, K. Tomizaki, K. Kajikawa, H. Mihara, Label and Label-Free Detection Techniques for Protein Microarrays, Microarrays. 4 (2015) 228–244. https://doi.org/10.3390/microarrays4020228.
[3] B. Aslam, M. Basit, M.A. Nisar, M. Khurshid, M.H. Rasool, Proteomics: Technologies and their applications, J. Chromatogr. Sci. 55 (2017) 182–196. https://doi.org/10.1093/chromsci/bmw167.
[4] X. Wang, Z. Ju, J. Huang, M. Hou, L. Zhou, C. Qi, Y. Zhang, Q. Gao, Q. Pan, G. Li, J. Zhong, C. Wang, The relationship between the variants of the bovine MBL2 gene and milk production traits, mastitis, serum MBL-C levels and complement activity, Vet. Immunol. Immunopathol. 148 (2012) 311–319. https://doi.org/10.1016/j.vetimm.2012.06.017.
[5] J.I. Boye, C. Barbana, Protein Processing in Food and Bioproduct Manufacturing and Techniques for Analysis, in: N.T. Dunford (Ed.), Food Ind. Bioprod. Bioprocess., First, John Wiley & Sons, Inc, 2012: pp. 85–113.
[6] H. Li, F. Zhang, H. Guo, Y. Zhu, J. Yuan, G. Yang, L. An, Molecular characterization of hepcidin gene in common carp (Cyprinus carpio L.) and its expression pattern responding to bacterial challenge, Fish Shellfish Immunol. 35 (2013) 1030–1038. https://doi.org/10.1016/j.fsi.2013.07.001.
[7] S.J. Shan, D.Z. Liu, L. Wang, Y.Y. Zhu, F.M. Zhang, T. Li, L.G. An, G.W. Yang, Identification and expression analysis of irak1 gene in common carp Cyprinus carpio L.: Indications for a role of antibacterial and antiviral immunity, J. Fish Biol. 87 (2015) 241–255. https://doi.org/10.1111/jfb.12714.
[8] H. Kaur, S.R. Bhagwat, T.K. Sharma, A. Kumar, Analytical techniques for characterization of biological molecules - Proteins and aptamers/oligonucleotides, Bioanalysis. 11 (2019) 103–117. https://doi.org/10.4155/bio-2018-0225.
[9] H. Chang, H. Kang, E. Ko, B.H. Jun, H.Y. Lee, Y.S. Lee, D.H. Jeong, PSA Detection with Femtomolar Sensitivity and a Broad Dynamic Range Using SERS Nanoprobes and an Area-Scanning Method, ACS Sensors. 1 (2016) 645–649. https://doi.org/10.1021/acssensors.6b00053.
[10] J. Zheng, J. Bai, Q. Zhou, J. Li, Y. Li, J. Yang, R. Yang, DNA-templated in situ growth of AgNPs on SWNTs: A new approach for highly sensitive SERS assay of microRNA, Chem. Commun. 51 (2015) 6552–6555. https://doi.org/10.1039/c5cc01003a.
[11] X. Zeng, Y. Yang, N. Zhang, D. Ji, X. Gu, J.M. Jornet, Y. Wu, Q. Gan, Plasmonic interferometer array biochip as a new mobile medical device for cancer detection, IEEE J. Sel. Top. Quantum Electron. 25 (2018). https://doi.org/10.1109/JSTQE.2018.2865418.
[12] J.D. Faix, Biomarkers of sepsis, Crit. Rev. Clin. Lab. Sci. 50 (2013) 23–36. https://doi.org/10.3109/10408363.2013.764490.
[13] H.J. Wang, P.J. Zhang, W.J. Chen, D. Feng, Y.H. Jia, L.X. Xie, Four serum microRNAs identified as diagnostic biomarkers of sepsis, J. Trauma Acute Care Surg. 73 (2012) 850–854. https://doi.org/10.1097/TA.0b013e31825a7560.
[14] M. Huang, H. Deng, J. Li, X. Tao, B. Jia, Exosomes in Sepsis Diagnosis and Treatment, Int. J. Clin. Med. 10 (2019) 565–575. https://doi.org/10.4236/ijcm.2019.1010046.
[15] Y.-C. Chen, W.-C. Shih, W.-T. Chang, C.-H. Yang, K.-S. Kao, C.-C. Cheng, Biosensor for human IgE detection using shear-mode FBAR devices, Nanoscale Res. Lett. 10 (2015) 69. https://doi.org/10.1186/s11671-015-0736-3.
[16] G. Sircar, B. Saha, S.G. Bhattacharya, S. Saha, Allergic asthma biomarkers using systems approaches, Front. Genet. 4 (2013) 1–10. https://doi.org/10.3389/fgene.2013.00308.
[17] B. Sastre, J.A. Cañas, J.M. Rodrigo-Muñoz, V. del Pozo, Novel modulators of asthma and allergy: Exosomes and microRNAs, Front. Immunol. 8 (2017) 1–14. https://doi.org/10.3389/fimmu.2017.00826.
[18] M.K. Mustafa, A. Nabok, D. Parkinson, I.E. Tothill, F. Salam, A. Tsargorodskaya,

Detection of beta amyloid peptide (1–16) and amyloid precursor protein (APP770) using spectroscopic ellipsometry and QCM techniques: A step forward towards Alzheimers disease diagnostics-amyloid peptide (1-16) and amyloid precursor protein (APP770) using , Biosens. Bioelectron. 26 (2010) 1332–1336. https://doi.org/10.1016/j.bios.2010.07.042.

[19] T. Smith-Vikos, F.J. Slack, MicroRNAs circulate around Alzheimer's disease., Genome Biol. 14 (2013) 125. https://doi.org/10.1186/gb4116.

[20] L. Jiang, H. Dong, H. Cao, X. Ji, S. Luan, J. Liu, Exosomes in pathogenesis, diagnosis, and treatment of alzheimer's disease, Med. Sci. Monit. 25 (2019) 3329–3335. https://doi.org/10.12659/MSM.914027.

[21] M.A. De Groote, D.G. Sterling, T. Hraha, T.M. Russell, L.S. Green, K. Wall, S. Kraemer, R. Ostroff, N. Janjic, U.A. Ochsner, Discovery and validation of a six-marker serum protein signature for the diagnosis of active pulmonary tuberculosis, J. Clin. Microbiol. 55 (2017) 3057–3071. https://doi.org/10.1128/JCM.00467-17.

[22] A. Chakraborty, S. Monica, Host biomarkers for early diagnosis of infectious diseases: A comprehensive review, Int. J. Clin. Microbiol. Biochem. Technol. 2 (2019) 001–007. https://doi.org/10.29328/journal.ijcmbt.1001005.

[23] S. Hadifar, A. Fateh, M.H. Yousefi, S.D. Siadat, F. Vaziri, Exosomes in tuberculosis: Still terra incognita?, J. Cell. Physiol. 234 (2019) 2104–2111. https://doi.org/10.1002/jcp.27555.

[24] W. Guo, Y. Hu, H. Wei, Enzymatically activated reduction-caged SERS reporters for versatile bioassays, Analyst. 142 (2017) 2322–2326. https://doi.org/10.1039/c7an00552k.

[25] C. Schulte, T. Zeller, microRNA-based diagnostics and therapy in cardiovascular disease-Summing up the facts., Cardiovasc. Diagn. Ther. 5 (2015) 17–36. https://doi.org/10.3978/j.issn.2223-3652.2014.12.03.

[26] G. Bellin, C. Gardin, L. Ferroni, J. Chachques, M. Rogante, D. Mitrečić, R. Ferrari, B. Zavan, Exosome in Cardiovascular Diseases: A Complex World Full of Hope, Cells. 8 (2019) 166. https://doi.org/10.3390/cells8020166.

[27] Y. Fu, D. Zhao, L. Yang, Protein-Based Biomarkers in Cerebrospinal Fluid and Blood for Alzheimer???s Disease, J. Mol. Neurosci. 54 (2014) 739–747. https://doi.org/10.1007/s12031-014-0356-x.

[28] B. Zimmermann, C. Hahnefeld, F.W. Herberg, B. Zimmermann, Applications of biomolecular interaction analysis in drug development, Targets. 1 (2002) 66–73. www.drugdiscoverytoday.com.

[29] C.A. Gedye, A. Hussain, J. Paterson, A. Smrke, H. Saini, D. Sirskyj, K. Pereira, N. Lobo, J. Stewart, C. Go, J. Ho, M. Medrano, E. Hyatt, J. Yuan, S. Lauriault, M. Kondratyev, T. Van Den Beucken, M. Jewett, P. Dirks, C.J. Guidos, J. Danska, J. Wang, B. Wouters, B. Neel, R. Rottapel, L.E. Ailles, Cell surface profiling using high-throughput flow cytometry: A platform for biomarker discovery and analysis of cellular heterogeneity, PLoS One. 9 (2014). https://doi.org/10.1371/journal.pone.0105602.

[30] H. Anderson, M. Jönsson, L. Vestling, U. Lindberg, T. Aastrup, Quartz crystal microbalance sensor design. I. Experimental study of sensor response and performance, Sensors Actuators, B Chem. 123 (2007) 27–34. https://doi.org/10.1016/j.snb.2006.07.027.

[31] B. Leca-Bouvier, B. Leca-Bouvier, L.J. Blum, L.J. Blum, Biosensors for protein detection: A review, Anal. Lett. 38 (2005) 1491–1517. https://doi.org/10.1081/AL-200065780.

[32] G. Selvolini, G. Marrazza, MIP-based sensors: Promising new tools for cancer biomarker determination, Sensors (Switzerland). 17 (2017). https://doi.org/10.3390/s17040718.

[33] A.C.L. Lee, J.L. Harris, K.K. Khanna, J.H. Hong, A comprehensive review on current advances in peptide drug development and design, Int. J. Mol. Sci. 20 (2019) 1–21. https://doi.org/10.3390/ijms20102383.

[34] J.C. Encarnação, T. Schulte, A. Achour, H. Björkelund, K. Andersson, Detecting

ligand interactions in real time on living bacterial cells, Appl. Microbiol. Biotechnol. 102 (2018) 4193–4201. https://doi.org/10.1007/s00253-018-8919-3.
[35] P.J. Molino, M.J. Higgins, P.C. Innis, R.M.I. Kapsa, G.G. Wallace, Fibronectin and bovine serum albumin adsorption and conformational dynamics on inherently conducting polymers: A QCM-D study, Langmuir. 28 (2012) 8433–8445. https://doi.org/10.1021/la300692y.
[36] K. Iha, M. Inada, N. Kawada, K. Nakaishi, S. Watabe, Y.H. Tan, C. Shen, L.Y. Ke, T. Yoshimura, E. Ito, Ultrasensitive ELISA developed for diagnosis, Diagnostics. 9 (2019) 1–9. https://doi.org/10.3390/diagnostics9030078.
[37] L.M. Ganova-Raeva, Y.E. Khudyakov, Application of mass spectrometry to molecular diagnostics of viral infections, Expert Rev. Mol. Diagn. 13 (2013) 377–388. https://doi.org/10.1586/erm.13.24.
[38] S.J. Opella, F.M. Marassi, Applications of NMR to membrane proteins, Arch. Biochem. Biophys. 628 (2017) 92–101. https://doi.org/10.1016/j.abb.2017.05.011.
[39] Y.F. Tian, C.F. Ning, F. He, B.C. Yin, B.C. Ye, Highly sensitive detection of exosomes by SERS using gold nanostar@Raman reporter@nanoshell structures modified with a bivalent cholesterol-labeled DNA anchor, Analyst. 143 (2018) 4915–4922. https://doi.org/10.1039/c8an01041b.
[40] G. Papadakis, P. Palladino, D. Chronaki, A. Tsortos, E. Gizeli, Sample-to-answer acoustic detection of DNA in complex samples, Chem. Commun. 53 (2017) 8058–8061. https://doi.org/10.1039/c6cc10175e.
[41] N. Bellassai, R. D'Agata, V. Jungbluth, G. Spoto, Surface Plasmon Resonance for Biomarker Detection: Advances in Non-invasive Cancer Diagnosis, Front. Chem. 7 (2019) 1–16. https://doi.org/10.3389/fchem.2019.00570.
[42] M. Vestergaard, K. Kerman, E. Tamiya, An Overview of Label-free Electrochemical Protein Sensors, Sensors. 7 (2007) 3442–3458. https://doi.org/10.3390/s7123442.
[43] D.M. Rissin, C.W. Kan, L. Song, A.J. Rivnak, M.W. Fishburn, Q. Shao, T. Piech, E.P. Ferrell, R.E. Meyer, T.G. Campbell, D.R. Fournier, D.C. Duffy, Multiplexed single molecule immunoassays., Lab Chip. 13 (2013) 2902–11. https://doi.org/10.1039/c3lc50416f.
[44] Z. Fu, Y.-C. Lu, J.J. Lai, Recent Advances in Biosensors for Nucleic Acid and Exosome Detection, Chonnam Med. J. 55 (2019) 86. https://doi.org/10.4068/cmj.2019.55.2.86.
[45] A. Bosco, E. Ambrosetti, J. Mavri, P. Capaldo, L. Casalis, Miniaturized aptamer-based assays for protein detection, Chemosensors. 4 (2016) 1–10. https://doi.org/10.3390/chemosensors4030018.
[46] B.N. Feltis, B.A. Sexton, F.L. Glenn, M.J. Best, M. Wilkins, T.J. Davis, A hand-held surface plasmon resonance biosensor for the detection of ricin and other biological agents, Biosens. Bioelectron. 23 (2008) 1131–1136. https://doi.org/10.1016/j.bios.2007.11.005.
[47] C.I. Cheng, Y.-P. Chang, Y.-H. Chu, Biomolecular interactions and tools for their recognition: focus on the quartz crystal microbalance and its diverse surface chemistries and applications, Chem. Soc. Rev. 41 (2012) 1947. https://doi.org/10.1039/c1cs15168a.
[48] C. Kößlinger, S. Drost, F. Aberl, H. Wolf, S. Koch, P. Woias, A quartz crystal biosensor for measurement in liquids, Biosens. Bioelectron. 7 (1992) 397–404. https://doi.org/10.1016/0956-5663(92)85038-C.
[49] M. Rodahl, B. Kasemo, Frequency and dissipation-factor responses to localized liquid deposits on a QCM electrode, Sensors Actuators B Chem. 37 (1996) 111–116. https://doi.org/10.1016/S0925-4005(97)80077-9.
[50] C. Chagnard, P. Gilbert, A.N. Watkins, T. Beeler, D.W. Paul, An electronic oscillator with automatic gain control: EQCM applications, Sensors Actuators, B Chem. 32 (1996) 129–136. https://doi.org/10.1016/0925-4005(96)80121-3.
[51] S.J. Martin, V.E. Granstaff, G.C. Frye, Characterization of a Quartz Crystal Microbalance with Simultaneous Mass and Liquid Loading, Anal. Chem. 2281 (1991)

2272–2281. https://doi.org/10.1021/ac00020a015.
[52] F. Höök, M. Rodahl, C. Keller, K. Glasmastar, C. Fredriksson, P. Dahiqvist, B. Kasemo, The dissipative QCM-D technique: interfacial phenomena and sensor applications for proteins, biomembranes, living cells and polymers, IEEE. 2 (1999) 966–972. https://doi.org/10.1109/FREQ.1999.841467.
[53] J. Petri, S. Hochstädt, T. Nentwig, A. Pausch, A. Langhoff, D. Johannsmann, A Fast Electrochemical Quartz Crystal Microbalance,which Acquires Frequency and Bandwidth on Multiple Overtones, Electroanalysis. 28 (2016) 1–9. https://doi.org/10.1002/elan.201600580.
[54] A. Guha, N. Sandström, V.P. Ostanin, W. van der Wijngaart, D. Klenerman, S.K. Ghosh, Simple and ultrafast resonance frequency and dissipation shift measurements using a fixed frequency drive, Sensors Actuators, B Chem. 281 (2019) 960–970. https://doi.org/10.1016/j.snb.2018.11.052.
[55] I.Y. Huang, M.C. Lee, Development of a FPW allergy biosensor for human IgE detection by MEMS and cystamine-based SAM technologies, Sensors Actuators, B Chem. 132 (2008) 340–348. https://doi.org/10.1016/j.snb.2008.01.048.
[56] Z. Li, Y. Yi, X. Luo, N. Xiong, Y. Liu, S. Li, R. Sun, Y. Wang, B. Hu, W. Chen, Y. Zhang, J. Wang, B. Huang, Y. Lin, J. Yang, W. Cai, X. Wang, J. Cheng, Z. Chen, K. Sun, W. Pan, Z. Zhan, L. Chen, F. Ye, Development and Clinical Application of A Rapid IgM-IgG Combined Antibody Test for SARS-CoV-2 Infection Diagnosis., J. Med. Virol. (2020) 0–1. https://doi.org/10.1002/jmv.25727.
[57] X. Su, F. Tim Chew, S.F.Y. Li, Piezoelectric quartz crystal based label-free analysis for allergy disease, Biosens. Bioelectron. 15 (2000) 629–639. https://doi.org/10.1016/S0956-5663(00)00112-3.
[58] C. Yao, T. Zhu, Y. Qi, Y. Zhao, H. Xia, W. Fu, Development of a quartz crystal microbalance biosensor with aptamers as bio-recognition element, Sensors. 10 (2010) 5859–5871. https://doi.org/10.3390/s100605859.
[59] C.-C. Chang, C.-Y. Chen, X. Zhao, T.-H. Wu, S.-C. Wei, C.-W. Lin, Label-free colorimetric aptasensor for IgE using DNA pseudoknot probe., Analyst. 139 (2014) 3347–51. https://doi.org/10.1039/c4an00253a.
[60] Y.M. Liu, J.J. Yang, J.T. Cao, J.J. Zhang, Y.H. Chen, S.W. Ren, An electrochemiluminescence aptasensor based on CdSe/ZnS functionalized MoS2 and enzymatic biocatalytic precipitation for sensitive detection of immunoglobulin e, Sensors Actuators, B Chem. 232 (2016) 538–544. https://doi.org/10.1016/j.snb.2016.03.165.
[61] B.G.G. Oliver, P. Robinson, M. Peters, J. Black, Viral infections and asthma: An inflammatory interface?, Eur. Respir. J. 44 (2014) 1666–1681. https://doi.org/10.1183/09031936.00047714.
[62] G. Proczek, A.-L. Gassner, J.-M. Busnel, H.H. Girault, Total serum IgE quantification by microfluidic ELISA using magnetic beads, Anal. Bioanal. Chem. 402 (2012) 2645–2653. https://doi.org/10.1007/s00216-011-5495-0.
[63] J.J. Garcia, M. Blanca, F. Moreno, J.M. Vega, C. Mayorga, J. Fernandez, C. Juarez, A. Romano, E. De Ramon, Determination of IgE antibodies to the benzylpenicilloyl determinant: A comparison of the sensitivity and specificity of three radio allergo sorbent test methods, J. Clin. Lab. Anal. 11 (1997) 251–257. https://doi.org/10.1002/(SICI)1098-2825(1997)11:5<251::AID-JCLA3>3.0.CO;2-A.
[64] K. Stadtherr, H. Wolf, P. Lindner, An aptamer-based protein biochip, Anal. Chem. 77 (2005) 3437–3443. https://doi.org/10.1021/ac0483421.
[65] M.D. Chapman, Lateral flow tests for allergy diagnosis: Point-of-care or point of contention?, Int. Arch. Allergy Immunol. 152 (2010) 301–302. https://doi.org/10.1159/000288282.
[66] S. Rahmatpour, A.H. Khan, R. Nasiri Kalmarzi, M. Rajabibazl, G. Tavoosidana, E. Motevaseli, N. Zarghami, E. Sadroddiny, Application of immuno-PCR assay for the detection of serum IgE specific to Bermuda allergen, Mol. Cell. Probes. 32 (2017) 1–4. https://doi.org/10.1016/j.mcp.2016.10.002.

[67] J.R. Cole, L.W.D. Jr, E.J. Morgan, L.B. Mcgown, Affinity Capture and Detection of Immunoglobulin E in Human Serum using an Aptamer-Modified Surface in Matrix Assisted Laser Desorption/Ionization Mass Spectrometry, Anal Chem. 79 (2007) 273–279. https://doi.org/10.1021/ac061256b.Affinity.
[68] D. Pomponi, M.L. Bernardi, M. Liso, P. Palazzo, L. Tuppo, C. Rafaiani, M. Santoro, A. Labrada, M.A. Ciardiello, A. Mari, E. Scala, Allergen micro-bead array for IgE detection: A feasibility study using allergenic molecules tested on a flexible multiplex flow cytometric immunoassay, PLoS One. 7 (2012) 1–16. https://doi.org/10.1371/journal.pone.0035697.
[69] B. Schweitzer, S. Wiltshire, J. Lambert, S. O'Malley, K. Kukanskis, Z. Zhu, S.F. Kingsmore, P.M. Lizardi, D.C. Ward, Immunoassays with rolling circle DNA amplification: a versatile platform for ultrasensitive antigen detection., Proc. Natl. Acad. Sci. U. S. A. 97 (2000) 10113–9. https://doi.org/10.1073/pnas.170237197.
[70] J.L. He, Z.S. Wu, S.B. Zhang, G.L. Shen, R.Q. Yu, Novel fluorescence enhancement IgE assay using a DNA aptamer, Analyst. 134 (2009) 1003–1007. https://doi.org/10.1039/b812450g.
[71] B. Teste, F. Malloggi, J.-M. Siaugue, A. Varenne, F. Kanoufi, S. Descroix, Microchip integrating magnetic nanoparticles for allergy diagnosis, Lab Chip. 11 (2011) 4207–4213. https://doi.org/10.1039/C1LC20809H.
[72] X. Su, J. Zhang, Comparison of surface plasmon resonance spectroscopy and quartz crystal microbalance for human IgE quantification, Sensors Actuators, B Chem. 100 (2004) 309–314. https://doi.org/10.1016/j.snb.2004.01.020.
[73] Y.H. Kim, J.P. Kim, S.J. Han, S.J. Sim, Aptamer biosensor for lable-free detection of human immunoglobulin E based on surface plasmon resonance, Sensors Actuators, B Chem. 139 (2009) 471–475. https://doi.org/10.1016/j.snb.2009.03.013.
[74] S. Kim, J. Lee, S.J. Lee, H.J. Lee, Ultra-sensitive detection of IgE using biofunctionalized nanoparticle-enhanced SPR, Talanta. 81 (2010) 1755–1759. https://doi.org/10.1016/j.talanta.2010.03.036.
[75] K.-J. Huang, Y.-J. Liu, J.-T. Cao, H.-B. Wang, An aptamer electrochemical assay for sensitive detection of immunoglobulin E based on tungsten disulfide-graphene composites and gold nanoparticles, RSC Adv. 4 (2014) 36742–36748. https://doi.org/10.1039/c4ra06133k.
[76] C.Y. Lee, K.Y. Wu, H.L. Su, H.Y. Hung, Y.Z. Hsieh, Sensitive label-free electrochemical analysis of human IgE using an aptasensor with cDNA amplification, Biosens. Bioelectron. 39 (2013) 133–138. https://doi.org/10.1016/j.bios.2012.07.009.
[77] Y.F. Liu, J.J. Tsai, Y.T. Chin, E.C. Liao, C.C. Wu, G.J. Wang, Detection of allergies using a silver nanoparticle modified nanostructured biosensor, Sensors Actuators, B Chem. 171–172 (2012) 1095–1100. https://doi.org/10.1016/j.snb.2012.06.039.
[78] D.T. Tran, V. Vermeeren, L. Grieten, S. Wenmackers, P. Wagner, J. Pollet, K.P.F. Janssen, L. Michiels, J. Lammertyn, Nanocrystalline diamond impedimetric aptasensor for the label-free detection of human IgE, Biosens. Bioelectron. 26 (2011) 2987–2993. https://doi.org/10.1016/j.bios.2010.11.053.
[79] A. Salimi, S. Khezrian, R. Hallaj, A. Vaziry, Highly sensitive electrochemical aptasensor for immunoglobulin e detection based on sandwich assay using enzyme-linked aptamer, Anal. Biochem. 466 (2014) 89–97. https://doi.org/10.1016/j.ab.2014.08.019.
[80] D. Xu, D. Xu, X. Yu, Z. Liu, W. He, Z. Ma, Label-free electrochemical detection for aptamer-based array electrodes, Anal. Chem. 77 (2005) 5107–5113. https://doi.org/10.1021/ac050192m.
[81] S. Khezrian, A. Salimi, H. Teymourian, R. Hallaj, Label-free electrochemical IgE aptasensor based on covalent attachment of aptamer onto multiwalled carbon nanotubes/ionic liquid/chitosan nanocomposite modified electrode, Biosens. Bioelectron. 43 (2013) 218–225. https://doi.org/10.1016/j.bios.2012.12.006.
[82] X. Luo, I. Lee, J. Huang, M. Yun, X.T. Cui, Ultrasensitive protein detection using an aptamer-functionalized single polyaniline nanowire., Chem. Commun. (Camb). 47

(2011) 6368–70. https://doi.org/10.1039/c1cc11353d.
[83] Y. Ohno, K. Maehashi, K. Matsumoto, Label-free biosensors based on aptamer-modified graphene field-effect transistors, J. Am. Chem. Soc. 132 (2010) 18012–18013. https://doi.org/10.1021/ja108127r.
[84] K. Maehashi, T. Katsura, K. Kerman, Y. Takamura, K. Matsumoto, E. Tamiya, Label-free protein biosensor based on aptamer-modified carbon nanotube field-effect transistors, Anal. Chem. 79 (2007) 782–787. https://doi.org/10.1021/ac060830g.
[85] M. Hasegawa, Y. Hirayama, Y. Ohno, K. Maehashi, K. Matsumoto, Characterization of reduced graphene oxide field-effect transistor and its application to biosensor, Jpn. J. Appl. Phys. 53 (2014). https://doi.org/10.7567/JJAP.53.05FD05.
[86] K. Maehashi, K. Matsumoto, Y. Takamura, Aptamer-Based Label-Free Immunosensors Using Carbon Nanotube Field-Effect Transistors, Electroanalysis. 21 (2009) 1285–1290. https://doi.org/10.1002/elan.200804552.
[87] X. Su, F. Chew, S.F.Y. Li, Self-assembled monolayer-based piezoelectric crystal immonosensor for the quantification of total human immunoglobulin E, Anal. Biochem. 273 (1999) 66–72.
[88] U. Schaible, M. Liss, E. Prohaska, J. Decker, K. Stadtherr, H. Wolf, Affinity measurements of biological molecules by a quartz crystal microbalance (QCM) biosensor., Methods Mol. Med. 94 (2004) 321–330. https://doi.org/10.1385/1592596797.
[89] M. Liss, B. Petersen, H. Wolf, E. Prohaska, An aptamer-based quartz crystal protein biosensor, Anal. Chem. 74 (2002) 4488–4495. https://doi.org/10.1021/ac011294p.
[90] C. Yao, Q. Chen, M. Chen, B. Zhang, Y. Luo, Q. Huang, J. Huang, W. Fu, A Novel Piezoelectric Quartz Micro-Array Immunosensor for Detection of ImmunoglobulinE, J. Nanosci. Nanotechnol. 6 (2006) 7. https://doi.org/http://dx.doi.org.wwwproxy0.library.unsw.edu.au/10.1166/jnn.2006.605.
[91] C. Yao, Y. Qi, Y. Zhao, Y. Xiang, Q. Chen, W. Fu, Aptamer-based piezoelectric quartz crystal microbalance biosensor array for the quantification of IgE, Biosens. Bioelectron. 24 (2009) 2499–2503. https://doi.org/10.1016/j.bios.2008.12.036.
[92] Y.-C. Chen, W.-T. Chang, C.-C. Cheng, J.-Y. Shen, K.-S. Kao, Development of human IgE biosensor using Sezawa-mode SAW devices, Curr. Appl. Phys. 14 (2014) 608–613. https://doi.org/10.1016/j.cap.2014.02.012.
[93] H.J. Lee, S.O. Jung, J.Y. Shim, Surface acoustic wave immunosensor for diagnosing allergy disease and method for diagnosing allergy disease using the same, 09150484.5, 2009. https://doi.org/10.1371/joumal.pone.0010853.
[94] I. Huang, M. Lee, Y. Chang, Development of a Novel Flexural Plate Wave Biosensor for Immunoglobulin-E Detection by Using SAM and MEMS Technologies, (2006) 70–73.
[95] G.T. Rozenblum, I.G. Pollitzer, M. Radrizzani, Challenges in electrochemical aptasensors and current sensing architectures using flat gold surfaces, Chemosensors. 7 (2019). https://doi.org/10.3390/chemosensors7040057.
[96] S. Mansouri, Miniaturization of Electrochemical Sensors, in: 17th Int. Meet. Chem. Sensors - IMCS 2018, Bedford MA, 2018: pp. 252–253. https://doi.org/10.5162/IMCS2018/EC3.2.
[97] A. Alassi, M. Benammar, D. Brett, Quartz crystal microbalance electronic interfacing systems: A review, Sensors (Switzerland). 17 (2017) 1–41. https://doi.org/10.3390/s17122799.
[98] I. German, D.D. Buchanan, R.T. Kennedy, Aptamers as ligands in affinity probe capillary electrophoresis., Anal. Chem. 70 (1998) 4540–4545. https://doi.org/10.1021/ac980638h.
[99] Q.W. Peng, Z.J. Cao, C.W. Lau, M. Kai, J.Z. Lu, Aptamer-barcode based immunoassay for the instantaneous derivatization chemiluminescence detection of IgE coupled to magnetic beads, Analyst. 136 (2011) 140–147. https://doi.org/Doi 10.1039/C0an00448k.

[100] G. Gokulrangan, J.R. Unruh, D.F. Holub, B. Ingram, C.K. Johnson, G.S. Wilson, DNA aptamer-based bioanalysis of IgE by fluorescence anisotropy, Anal. Chem. 77 (2005) 1963–1970. https://doi.org/10.1021/ac0483926.
[101] T. Hianik, Affinity Biosensors for Detection Immunoglobulin E and Cellular Prions. Antibodies vs. DNA Aptamers, Electroanalysis. 28 (2016) 1764–1776. https://doi.org/10.1002/elan.201600153.
[102] B. Jiang, F. Li, C. Yang, J. Xie, Y. Xiang, R. Yuan, Aptamer pseudoknot-functionalized electronic sensor for reagentless and single-step detection of immunoglobulin e in human serum, Anal. Chem. 87 (2015) 3094–3098. https://doi.org/10.1021/acs.analchem.5b00041.
[103] K.J. Feng, C.H. Sun, J.H. Jiang, R.Q. Yu, An Aptamer-Based Competitive Fluorescence Quenching Assay for Ige, Anal. Lett. 44 (2011) 1301–1309. https://doi.org/Doi 10.1080/00032719.2010.511747.
[104] W. Song, H. Li, H. Liu, Z. Wu, W. Qiang, D. Xu, Fabrication of streptavidin functionalized silver nanoparticle decorated graphene and its application in disposable electrochemical sensor for immunoglobulin e, Electrochem. Commun. 31 (2013) 16–19. https://doi.org/10.1016/j.elecom.2013.02.001.
[105] C. da Silva Granja, N. Sandström, I. Efimov, V.P. Ostanin, W. van der Wijngaart, D. Klenerman, S.K. Ghosh, Characterisation of particle-surface interactions via anharmonic acoustic transduction, Sensors Actuators, B Chem. 272 (2018) 175–184. https://doi.org/10.1016/j.snb.2018.05.016.
[106] J.L. Casteleiro-Roca, J.L. Calvo-Rolle, M.C. Meizoso-Lopez, A. Pi˜nón-Pazos, B.A. Rodríguez-Gómez, New approach for the QCM sensors characterization, Sensors Actuators, A Phys. 207 (2014) 1–9. https://doi.org/10.1016/j.sna.2013.12.002.
[107] C. da S. Granja, K. Glen, N. Sandström, V.P. Ostanin, R.J. Thomas, S.K. Ghosh, A quartz crystal resonator for cellular phenotyping, Biosens. Bioelectron. X. 6 (2020). https://doi.org/10.1016/j.biosx.2020.100057.
[108] S. Khobragade, C. Da Silva Granja, N. Sandström, I. Efimov, V.P. Ostanin, W. van der Wijngaart, D. Klenerman, S.K. Ghosh, Direct detection of whole bacteria using a nonlinear acoustic resonator, Sensors Actuators, B Chem. 316 (2020). https://doi.org/10.1016/j.snb.2020.128086.
[109] G. Sauerbrey, Verwendung von Schwingquarzen zur Wägung dünner Schichten und zur Mikrowägung, Zeitschrift Für Phys. 155 (1959) 206–222. https://doi.org/10.1007/BF01337937.
[110] D. Johannsmann, L.O. Heim, A simple equation predicting the amplitude of motion of quartz crystal resonators, J. Appl. Phys. 100 (2006). https://doi.org/10.1063/1.2359138.
[111] F. Schwesinger, R. Ros, T. Strunz, D. Anselmetti, H.J. Güntherodt, A. Honegger, L. Jermutus, L. Tiefenauer, A. Plückthun, Unbinding forces of single antibody-antigen complexes correlate with their thermal dissociation rates, Proc. Natl. Acad. Sci. U. S. A. 97 (2000) 9972–9977. https://doi.org/10.1073/pnas.97.18.9972.
[112] V.H. Carvalho-Silva, N.D. Coutinho, V. Aquilanti, Temperature dependence of rate processes beyond Arrhenius and eyring: Activation and transitivity, Front. Chem. 7 (2019) 1–11. https://doi.org/10.3389/fchem.2019.00380.
[113] J. V Garcia, Y. Jimenez, C. March, A. Montoya, A. Arnau, QCM technology in biosensors, Biosens. - Emerg. Mater. Appl. (2011) 153–178. https://doi.org/10.5772/17991.
[114] X. Huang, Q. Chen, W. Pan, J. Hu, Y. Yao, Assessing the Mass Sensitivity for Different Electrode Materials Commonly Used in Quartz Crystal Microbalances (QCMs), Sensors (Basel). 19 (2019) 1–7. https://doi.org/http://dx.doi.org/10.3390/s19183968.
[115] X. Huang, Q. Bai, W. Pan, J. Hu, Quartz Crystal Microbalance with Approximately Uniform Sensitivity Distribution, Anal. Chem. (2018). https://doi.org/10.1021/acs.analchem.8b01529.
[116] J.M. Beechem, Multi-emission wavelength picosecond time-resolved fluorescence

decay data obtained on the millisecond time scale: Application to protein:DNA interactions and protein folding reaction, Time-Resolved Laser Spectrosc. Biochem. III- SPIE. 1640 (1992) 676–680.
[117] A. Rojnuckarin, S. Kim, S. Subramaniam, Brownian dynamics simulations of protein folding: Access to milliseconds time scale and beyond, Proc Natl Acad Sci U S A. 95 (1998) 4288–4292. https://doi.org/10.1073/pnas.95.8.4288.
[118] J. Schröder, R. Borngräber, F. Eichelbaum, P. Hauptmann, Advanced interface electronics and methods for QCM, Sensors Actuators, A Phys. 97–98 (2002) 543–547. https://doi.org/10.1016/S0924-4247(02)00036-5.
[119] S. Beißner, J.W. Thies, C. Bechthold, P. Kuhn, B. Thürmann, S. Dübel, A. Dietzel, Low-cost, in-liquid measuring system using a novel compact oscillation circuit and quartz-crystal microbalances (QCMs) as a versatile biosensor platform, J. Sensors Sens. Syst. 6 (2017) 341–350. https://doi.org/10.5194/jsss-6-341-2017.
[120] C. Mista, M. Zalazar, A. Pealva, M. Martina, J.M. Reta, Open Source Quartz Crystal Microbalance with dissipation monitoring, J. Phys. Conf. Ser. 705 (2016). https://doi.org/10.1088/1742-6596/705/1/012008.
[121] S. Saha, M. Raje, C.R. Suri, Sandwich microgravimetric immunoassay: Sensitive and specific detection of low molecular weight analytes using piezoelectric quartz crystal, Biotechnol. Lett. 24 (2002) 711–716. https://doi.org/10.1023/A:1015238201367.
[122] A. Jbari, L. Bellarbi, N. Zine, C.A. Mills, J. Samitier, A. Errachid, Multiplexed frequency spectrum analyzer instrumentation for the characterization of multiple QCM-based biosensors, 2007 Int. Conf. Sens. Technol. Appl. SENSORCOMM 2007, Proc. (2007) 436–440. https://doi.org/10.1109/SENSORCOMM.2007.4394960.
[123] C.A. Mills, K.T.C. Chai, M.J. Milgrew, A. Glidle, J.M. Cooper, D.R.S. Cumming, A multiplexed impedance analyzer for characterizing polymer-coated QCM sensor arrays, IEEE Sens. J. 6 (2006) 996–1001. https://doi.org/10.1109/JSEN.2006.877936.
[124] H. Shen, T. Zhou, J. Hu, A high-throughput QCM chip configuration for the study of living cells and cell-drug interactions, Anal. Bioanal. Chem. 409 (2017) 6463–6473. https://doi.org/10.1007/s00216-017-0591-4.
[125] M.E. Yakovleva, G.R. Safina, B. Danielsson, A study of glycoprotein-lectin interactions using quartz crystal microbalance, Anal. Chim. Acta. 668 (2010) 80–85. https://doi.org/10.1016/j.aca.2009.12.004.
[126] K. Jaruwongrungsee, U. Waiwijit, A. Wisitsoraat, M. Sangworasil, C. Pintavirooj, A. Tuantranont, Real-time multianalyte biosensors based on interference-free multichannel monolithic quartz crystal microbalance, Biosens. Bioelectron. 67 (2015) 576–581. https://doi.org/10.1016/j.bios.2014.09.047.
[127] A. Tuantranont, A. Wisitsora-at, P. Sritongkham, K. Jaruwongrungsee, A review of monolithic multichannel quartz crystal microbalance: A review, Anal. Chim. Acta. 687 (2011) 114–128. https://doi.org/10.1016/j.aca.2010.12.022.
[128] H. Ogi, H. Nagai, Y. Fukunishi, T. Yanagida, M. Hirao, M. Nishiyama, Multichannel wireless-electrodeless quartz-crystal microbalance immunosensor, Anal. Chem. 82 (2010) 3957–3962. https://doi.org/10.1021/ac100527r.
[129] W. Tao, P. Lin, Y. Ai, H. Wang, S. Ke, X. Zeng, Multichannel quartz crystal microbalance array: Fabrication, evaluation, application in biomarker detection, Anal. Biochem. 494 (2016) 85–92. https://doi.org/10.1016/j.ab.2015.11.001.
[130] X. Jin, Y. Huang, A. Mason, X. Zeng, Multichannel Monolithic Quartz Crystal Microbalance Gas Sensor Array, Anal. Chem. 81 (2009) 595–603. https://doi.org/10.1021/ac8018697.
[131] Y.-Y. Chen, L.-C. Huang, T.-T. Wu, J.-H. Sun, Isolation of bulk acoustic waves in a sensor array with phononic crystals, 2011 IEEE Int. Ultrason. Symp. (2011) 2487–2490. https://doi.org/10.1109/ULTSYM.2011.0618.
[132] H.H. Lu, Y.K. Rao, T.Z. Wu, Y.M. Tzeng, Direct characterization and quantification of volatile organic compounds by piezoelectric module chips sensor, Sensors Actuators, B Chem. 137 (2009) 741–746. https://doi.org/10.1016/j.snb.2009.01.060.
[133] D. Croux, A. Weustenraed, P. Pobedinskas, F. Horemans, H. Diliën, K. Haenen, T.

Cleij, P. Wagner, R. Thoelen, W. De Ceuninck, Development of multichannel quartz crystal microbalances for MIP-based biosensing, Phys. Status Solidi Appl. Mater. Sci. 209 (2012) 892–899. https://doi.org/10.1002/pssa.201100715.
[134] C. Garcia-Hernandez, C. Medina-Plaza, C. Garcia-Cabezon, F. Martin-Pedrosa, I. Del Valle, J.A. de Saja, M.L. Rodríguez-Méndez, An electrochemical quartz crystal microbalance multisensor system based on phthalocyanine nanostructured films: Discrimination of musts, Sensors (Switzerland). 15 (2015) 29233–29249. https://doi.org/10.3390/s151129233.
[135] G.S. Huang, M. Te Wang, M.Y. Hong, A versatile QCM matrix system for online and high-throughput bio-sensing, Analyst. 131 (2006) 382–387. https://doi.org/10.1039/b515722f.